European Journal of Mechanics A/Solids 29 (2010) 7–17

Contents lists available at ScienceDirect

European Journal of Mechanics A/Solids

journal homepage: www.elsevier.com/locate/ejmsol

Modeling on mass abrasion of kinetic energy penetrator

X.W. Chen [a,*], L.L. He [b], S.Q. Yang [a]

[a] Institute of Structural Mechanics, China Academy of Engineering Physics, P.O. Box 919-401, Mianyang, Sichuan 621900, China
[b] Department of Modern Mechanics, University of Science and Technology of China, Hefei, Anhui 230027, China

ARTICLE INFO

Article history:
Received 10 December 2008
Accepted 18 July 2009
Available online 6 August 2009

Keywords:
Mass loss
Kinetic energy penetrator
Penetration
Engineering model

ABSTRACT

An engineering model on mass abrasion of kinetic energy penetrator is presented to predict the nose shape and mass loss of the residual projectile after high-speed penetration into concrete. The experimental analysis indicates that the kinetic energy of penetrator (i.e., mass and velocity of projectile) and the hardness of aggregate of concrete significantly affect the mass abrasion of projectile. A theoretical upper limit exists for the mass loss. More general relationship between mass loss and impact function I of projectile is constructed. Graphical discussion declares that the most mass loss occurs on the nose of the projectile and the eroding nose approaches to an ogival shape with a smaller value of caliber-radius-head (CRH). A relative rate of mass abrasion on ogive-nose is further defined and analyzed. The mass loss from abrasion on kinetic energy (KE) penetrator may be evaluated through the variation of nose shape.

© 2009 Elsevier Masson SAS. All rights reserved.

1. Introduction

Earth penetration weapon (EPW) is applicable for attacking the underground targets protected by reinforced concrete and rocks. During a penetration process, enormous resistant force is applied on the outer surface of the projectile by the target medium. The penetration resistance of the target medium determines the terminal ballistics of the projectile as well as the deformation and damage of the projectile. The structural design of the projectile must be especially concerned to ensure the integrity of projectile during penetration process. Although the theoretical analysis usually treats the projectile as non-deformable to study the penetration/perforation of EPW, this is often inaccurate unrealistic due to the mass abrasion of the penetrator. Mass abrasion changes the nose shape and geometry of penetrator, and thus affects the penetration efficiency. With the research interests transferring from the conventional EPW (penetration velocity $V_i < 900$ m/s) to advanced EPW (1200 m/s $< V_i <$ 1500 m/s), the mass loss of KE penetrator becomes unavoidable, which significantly decreases the penetration efficiency and affects the structural design of projectiles. The abrasion may induce the instability of terminal ballistics of penetrator, and lead to the damage or failure of projectiles. The mass abrasion of penetrator is quite closely related to the structural design and optimization of high-speed KE penetrator. This aspect already becomes a focus topic among the international research communities (Forrestal et al., 1996; Frew et al., 1998; Jones et al., 2001, 2002; Silling and Forrestal, 2007; Klepaczko and Hughes, 2005; Beissel and Johnson, 2000, 2002; Davis et al., 2004; Jones et al., 2003).

The mass abrasion of projectile has already been observed in experiments of projectiles penetrating into concrete targets. Local abrasion and melting on the projectiles' surfaces have been surveyed in experiments by Forrestal et al. (1996) and Frew et al. (1998). The mass loss is localized in a thin film of exterior surface of projectile, such as the nose and shank. The ogive-nose becomes blunt, and its mass loss is up to 7%. Forrestal et al. (1996) quantitatively measured the mass loss of projectile after penetration. Jones et al. (2001, 2002) also reported some evaluation of mass loss during steel projectiles penetrating into concrete. In general, although there are some experimental data of mass loss of projectile impacting concrete, the systematic database of mass erosion of KE penetrators on different targets is still in construct (Silling and Forrestal, 2007).

In order to study the mass abrasion of projectile, the interaction between projectile-target (e.g. concrete and rock targets) surface should be well understood. Not only the projectile material (Here mainly focusing on high-strength alloy steels, e.g. AF1410, AISI4340, AerMet100, etc.) but also the target material (e.g. concrete, rocks and granular materials (sand, soil, etc.)) should be concerned. The characteristics of aggregate in concrete may also make the mechanism of mass abrasion more complicated. The related research on mass abrasion of projectile usually includes two aspects (Klepaczko and Hughes, 2005). One aspect is the theoretical and experimental investigation of dynamic friction on the surface between penetrator

* Corresponding author. Tel.: +86 816 2484434; fax: +86 816 2281485.
E-mail address: chenxiaoweintu@yahoo.com (X.W. Chen).

0997-7538/$ – see front matter © 2009 Elsevier Masson SAS. All rights reserved.
doi:10.1016/j.euromechsol.2009.07.006

and target, which mainly focuses on the variation of friction-coefficient, or more generally on the friction depending on the surface roughness in dynamic plasticity. The other aspect is the mass abrasion and erosion under extreme loading conditions. For the material being considered in this paper, the projectile nose experiences extreme high pressure and temperature during high-speed penetration, e.g., at velocity in range of 1200 m/s and 1500 m/s. It results in the mass abrasion of projectile and the mass abrasion process will occur over the duration of the penetration event, which accompanied with some physical and chemical phenomenon, e.g., material melting, phase transition, oxidation of metal scraped from the projectile surface and chemical reaction with target particles, and so on. Actually they all contribute to the mass loss of projectile. A systematic study of mass abrasion is beneficial for optimizing the ballistic performance of projectile under different conditions (Silling and Forrestal, 2007).

The nose of a KE penetrator undergoes high pressure and temperature during high-speed penetration, and is usually called as a critical zone. The mass abrasion depends on the material flow and chemical reactions at that critical zone. Micro-metallographical analysis and SEM indicate that, the projectile surface goes from high-temperature heating, melting to cool-down along with phase transition after penetration, which is shown as "white bands" with hardness more than 60HRC. Heat affected zone (HAZ) with a thickness between 20 and 100 μm is usually formed in the exterior surface of projectile, and it also has a high hardness. It indicates that penetrator material is heated upwards to austenite transition temperature and then quenched.

Beissel and Johnson (2000, 2002) constructed an axisymmetrical and a 3D FEA models for mass abrasion of projectile, respectively. The basic assumption of these models is, the rate of mass loss of projectile is proportional to the normal stress on the surface and the relative sliding velocity on projectile-target surface. In general, the models are convenient to evaluate the total mass abrasion of projectile but not in good agreement with the experimental observations for the nose shape. Since the model postulates that the mass abrasion mostly occurs in projectile shank, the nose shape after abrasion predicted by Beissel and Johnson (2000, 2002) is much sharper than the actuality. Based on the penetration experimental data reported before by Forrestal et al. (1996) and Frew et al. (1998), Silling and Forrestal (2007) found there exists a linear relation between the mass abrasion and the initial kinetic energy of projectile. Different from Beissel and Johnson (2000, 2002), Silling and Forrestal (2007) further assumed that the rate of mass abrasion on projectile surface was proportional to the penetration velocity and the axial resistant force. This model has been applied in the Eulerian hydrodynamic code CTH, which developed by Sandia National Lab, and an excellent agreement with the experimental observation enhances its rationality.

By means of normalized different-scale experimental data, Klepaczko and Hughes (2005) defined the universal parameters of the rate of wear and the rate sensitivity of wear, and constructed an effective method for analyzing the rate of mass abrasion. They further indicated that the mass abrasion mostly occurred on the nose of projectile and a little on projectile shank based on tests.

In the present paper, experimental data reported by Forrestal et al. (1996) and Frew et al. (1998) are further analyzed and the phenomena of projectile mass abrasion is graphically discussed. A more general relation between the projectile mass abrasion and impact function I is constructed.

2. Main factors affecting projectile mass abrasion

Forrestal et al. (1996) and Frew et al. (1998) conducted penetration experiments into concrete and grout targets with different high-strength alloy steel and different geometry projectiles, respectively. The mass loss of projectile had been recorded as well in these tests. Based on which, Klepaczko and Hughes (2005), Beissel and Johnson (2000, 2002) and Silling and Forrestal (2007) analyzed the mass abrasion of penetration projectiles, and suggested different numerical and theoretical models, respectively. Especially, Silling and Forrestal (2007) indicated that the projectile mass abrasion is linear proportional to the kinetic energy of projectile when the impact velocity is less than 1000 m/s. Therein an abrasion model depending on both of the normal stress and tangential stress on the projectile surface is constructed. The numerical results are in good agreement with tests. It is the most successful model for predicting projectile mass abrasion up to date. Referring to this paper, the present paper further summarizes all experimental data from Forrestal et al. (1996) and Frew et al. (1998) and aims to find the main factors affecting the projectile mass abrasion.

Table 1
Parameters of high-strength alloy steel penetrators penetrating into grout and concrete targets.

	Case 1	Case 2	Case 3	Case 4	Case 5	Case 6
Targets						
Target material	Grout	Grout	Concrete	Concrete	Concrete	concrete
Uniaxial compressive strength of concrete f_c (MPa)	13.5	21.6	62.8	51	58.4	58.4
Density ρ_t (kg/m^3)	2000	2000	2300	2300	2320	2320
Characteristic size of aggregate a (mm)	4.8	4.8	9.5	9.5	9.5	9.5
Aggregate material and Moh's hardness	Quartz 7.0	Quartz 7.0	Quartz 7.0	Quartz 7.0	Limestone 3.0	Limestone 3.0
S	19.6	15.5	9.1	10.1	9.42	9.42
Projectiles						
Geometry	Projectile with hollow shank and ogive-nose		Projectile with solid shank and ogive-nose			
Caliber-head-radius(CRH)	3.0 or 4.25	3.0 or 4.25	3.0	3.0	3.0	3.0
Mass M (g)	64	64	478	1600	478	1620
Mass of nose M_n (g)	12.0 or 14.3	12.0 or 14.3	46.8	158.7	46.8	158.7
M/M_n	5.3 or 4.5	5.3 or 4.5	10.2	10.1	10.2	10.2
Shank diameter d (mm)	12.9	12.9	20.3	30.5	20.3	30.5
Length-to-diameter ratio L/d	6.88	6.88	10	10	10	10
d/a	2.69	2.69	2.14	3.21	2.14	3.21
geometry function N of prototype projectiles	143.4 or 200	143.4 or 200	234.3	231.3	232.4	232.2
Minimum geometry function N_r of residual projectiles after test	–	58.0 $CRH_{min} = 1.25$	46.4 $CRH_{min} = 0.5$	45.7 $CRH_{min} = 0.5$	80.6 $CRH_{min} = 1.0$	95.4 $CRH_{min} = 1.2$
Projectile material and hardness R_c	4340 R_c39	4340 R_c39	4340 R_c45	4340 R_c45	4340 R_c45 AerMet 100 R_c 53	4340 R_c45 AerMet 100 R_c 53

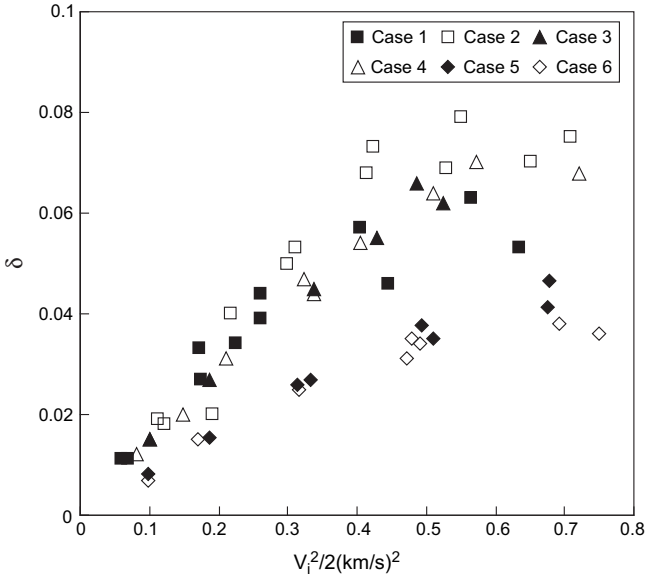

Fig. 1. Relation between the mass loss of projectiles and the initial impact velocity.

There are total six-set experiments of different high-strength alloy projectiles penetrating into grout and concrete targets in Forrestal et al. (1996) and Frew et al. (1998). The parameters of projectiles and targets possibly relating to the mass abrasion are listed in Table 1, in which Cases 1–4 are reported by Forrestal et al. (1996) and Cases 5–6 by Frew et al. (1998).

Fig. 1 shows the mass loss of projectiles of all six-set experiments in Forrestal et al. (1996) and Frew et al. (1998) with the initial impact velocity. Obviously, just as indicated by Silling and Forrestal (2007), when impact velocities are less than 1000 m/s [or $V_i^2/2 \le 0.5(\text{km/s})^2$], the relation between mass abrasion and kinetic energy of projectile is linear; while when impact velocities higher than 1000 m/s, projectile mass abrasion maintains as constant. The rate of mass abrasion δ can be expressed by the empirical formulae as follows:

$$\delta = \frac{\Delta M}{M} = \begin{cases} kV_i^2/2 & V_i \le 1 \text{ km/s} \\ C & V_i > 1 \text{ km/s} \end{cases} \quad (1)$$

where ΔM is the mass loss of projectile, and k and C are constants. Specially, $k_1 = 0.14$ and $C_1 = 0.07$ for Cases 1–4 (Forrestal et al., 1996); while $k_2 = 0.07$ and $C_2 = 0.035$ for Cases 5–6 (Frew et al., 1998).

The different experimental conditions are analyzed and the details are listed in Table 1, respectively. According to Table 1 and Fig. 1, although the strength and density of concrete, size of aggregate, and the nose shape and geometry of projectile are distinctly different from Case 1 to Case 4, the linear relations between the mass abrasion of projectile and the initial kinetic energy of projectile are approximately the same. Cases 5–6 are in like manner, and in particular the projectile materials are different. It indicates that when a projectile made of high-strength alloy steel (i.e. AF1410, AISI4340, AerMet100, etc.) penetrating into concrete, the effects of the strength and density of concrete, size of aggregate, and the nose shape and geometry of projectile on the mass abrasion of projectile perhaps obey the same rules and an empirical prediction like Silling and Forrestal (2007) can be executed to evaluate the mass erosion at a macro-view.

The following question is that, why the linear relations (i.e., the coefficients k and C in Eq. (1)) are different regarding Cases 1–4 and Cases 5–6, respectively? One interesting observation from Table 1 is that, two kinds of aggregate are employed in the concrete targets of Cases 1–4 and Cases 5–6, respectively. Quartz aggregate is used in Cases 1–4 and its Moh's hardness H_1 is 7 (Forrestal et al., 1996), while limestone in Cases 5–6 and Moh's hardness H_2 is 3 (Frew et al., 1998). The ratio of aggregate hardness $H_1/H_2 = 2.33$, and it is quite similar to the ratios of the parameters of Eq. (1), i.e., $k_1/k_2 = 2.0$ and $C_1/C_2 = 2.0$.

It is reasonable to assume that the aggregate hardness of concrete affects the mass abrasion of projectile. Following this idea, the experimental data of mass loss δ of projectiles in Cases 5–6 are all modified by multiplying a factor $H_1/H_2 = 2.33$. The relation between the modified mass loss δ of projectiles and impact kinetic energy is reevaluated and shown in Fig. 2. It can be seen that all data distribute coincidently, and Eq. (1) is still correct, thus $k = 0.14$ and $C = 0.07$. Fig. 2 further confirms that the mass

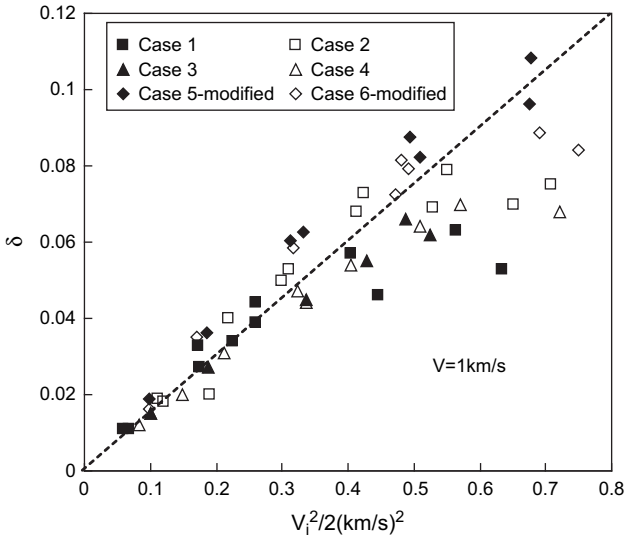

Fig. 2. Modification on the relation of Fig. 1 with accounting for the effect of aggregate.

abrasion of projectile significantly depends on the aggregate hardness.

Although mass abrasion exists, the basic geometric profile of a projectile is not changed during high-speed penetration. The non-deformable assumption is always employed in the theoretical analysis. Therein the relation between the mass abrasion and the impact function I of projectile is further discussed for examining the main factors affecting projectile mass abrasion.

Chen and Li (2002) and Li and Chen (2003) indicated that the penetration of rigid projectile is mainly dominated by two dimensionless numbers, i.e., the impact function I and geometry function N of projectile. For concrete target, the semi-empirical definitions are as follows,

$$I = \frac{MV_i^2}{d^3 S f_c}, \tag{2a}$$

$$N = \frac{M}{N^* \rho d^3} \tag{2b}$$

where M, d and V_i are the mass, shank diameter and initial impact velocity of projectile, respectively. ρ and f_c are the density and unconfined compressive strength of concrete target, respectively. S is a dimensionless empirical constant which related to the unconfined compressive strength f_c, i.e., $S = 82.6 f_c^{-0.544}$ or $S = 72.0 f_c^{-0.5}$ (where f_c in MPa unit). N^* is defined as the nose factor for depicting the influence of the geometry of rigid projectile on penetration.

As indicated in Chen and Li (2002) and Li and Chen (2003), the penetration depends mostly on the impact function I rather than the geometry function N of projectile. When the geometry function N is large enough, saying $N > 100$, which usually corresponding to a sharper and slender penetrator, the influence of N on penetration can be neglected. Table 1 also lists all the values of geometry function N of prototype projectiles and residual projectiles after test. Obviously, the values of the geometry function N of prototype projectiles are all greater than 100. It concludes that the shape of prototype projectiles is optimized enough and thus the influence of N on penetration is no need to discuss here.

In particular, the minimum value of the geometry function N of residual projectiles after test is still large enough. As listed in Table 1, we have $40 < N_r^{\mathrm{Min}} < 100$, and it confirms that the assumption of non-deformable projectile is still applicable. The formula

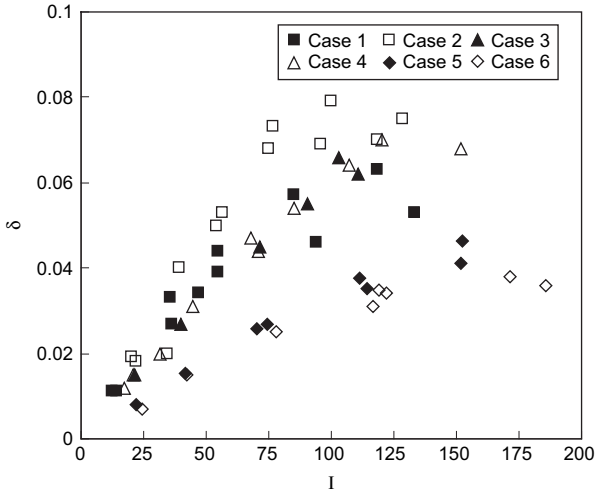

Fig. 3. Relation between the mass loss of projectiles and the impact function I of projectile.

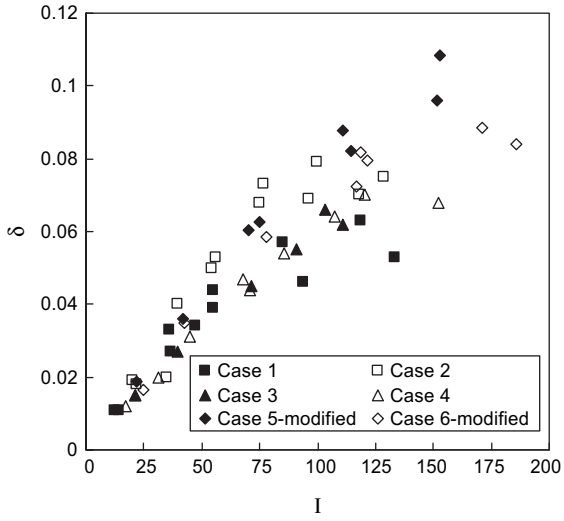

Fig. 4. Modification on the relation of Fig. 3 with accounting for the effect of aggregate.

$X/d = I/2$, previously reported by Chen and Li (2002) and Li and Chen (2003), still can be employed to evaluate the depth of penetration.

The relations of the rate of mass abrasion δ with the impact function I of projectile are depicted in Fig. 3 based on the experimental data of Forrestal et al. (1996) and Frew et al. (1998). The relations of the modified rate of mass abrasion δ with the impact function I of projectile are also demonstrated in Fig. 4. Similar to Fig. 2, the rate of mass abrasion of Cases 5–6 is multiplied by a factor $H_1/H_2 = 2.33$ in Fig. 4.

As we can see from Table 2, Figs. 3 and 4 have a little data scattering with comparing to Figs. 1 and 2, but the linear relation is approximately maintained,

$$\delta = \frac{\Delta M}{M} = \begin{cases} k'I & I \le 120 \\ C' & I > 120 \end{cases} \tag{3}$$

In Fig. 3, we have $k'_1 = 5.83 \times 10^{-4}$ and $C'_1 = 0.07$ for cases 1–4 (Forrestal et al., 1996), while $k'_1 = 2.92 \times 10^{-4}$ and $C'_2 = 0.035$ for cases 5–6 (Frew et al., 1998). After accounting for the effect of aggregate and modified by multiplying a factor $H_1/H_2 = 2.33$, only an unique linear relation between the mass abrasion and the impact function is observed for all 6 cases and we have $k' = 5.83 \times 10^{-4}$ and $C' = 0.07$ in Fig. 4.

Except for the aggregate, the effects of concrete strength and density, the projectile nose shape, geometry and mass as well as the initial impact velocity (or the initial kinetic energy) have been already taken into account in Eqs. (2a) and (2b). It is believed that the slight data scattering of Figs. 3 and 4 is synthetically caused by the different concrete strength, density, aggregate and projectile material and geometry with comparing to Figs. 1 and 2.

In other words, Figs. 3 and 4 further confirm that the mass abrasion of a high-strength alloy steel projectile is significantly

Table 2
Standard deviation of linear fitting of experimental data.

	X	Y	Standard Deviation
Cases 1-4 in Figs. 1 and 3	$V_i^2/2$	δ	0.0062
	I	δ	0.0106
Cases 5-6 in Figs. 1 and 3	$V_i^2/2$	δ	0.0378
	I	δ	0.0394
Cases 1-6 in Figs. 2 and 4	$V^2/2$	δ	0.0084
	I	δ	0.0121

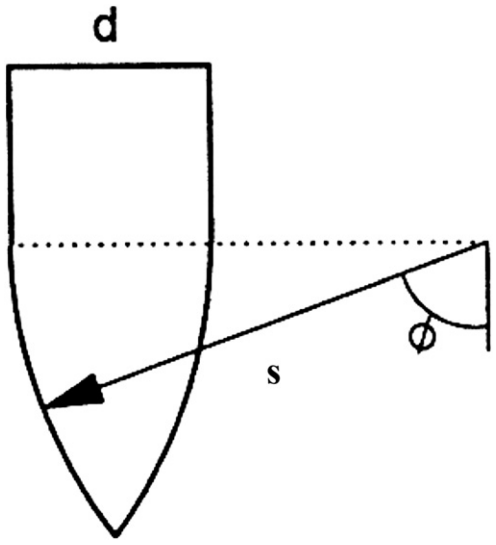

Fig. 5. Ogive nose geometry.

influenced by the initial impact velocity and aggregate hardness of concrete. The other factors, such as the concrete strength and density, aggregate size, projectile material and geometry and so on, have limited influence on the mass abrasion of projectile.

3. Mass abrasion of projectile and the variation of nose shape

The total mass abrasion of a projectile includes the mass loss on both its nose and shank. The mechanism of interaction of projectile-target surface should be well understood. The mass loss on the nose is caused by the flow erosion under extreme high pressure and temperature, while the mass loss on shank mostly comes from the sliding friction. As observed in Forrestal et al. (1996) and Frew et al. (1998), the majority of the mass loss occurred on the nose of projectile.

In the numerical simulations of Beissel and Johnson (2000, 2002), they predicted that mass abrasion mostly occurred on the shank of projectile and the projectile became much sharper. However, this is inconsistent with the experimental results. Comparatively, the simulation by Silling and Forrestal (2007) agrees well with the tests, and one of the most important conclusions is that the mass abrasion mostly takes place on the nose of projectile.

In this section, the relation between the mass abrasion of projectile and the variation of nose shape is further discussed. The ogive-nose projectiles are usually employed in deep penetration. According to Forrestal et al. (1996) and Frew et al. (1998), we notice that the nose shape of the residual projectile after penetration is still ogival but with a smaller value of caliber-radius-head (CRH) than prototype's. Therein it is possible to estimate the mass loss of the nose of projectile through evaluating the volume change of projectile nose. Here we assume the nose part of projectile is elemental solid.

As shown in Fig. 5, the volume of the ogive nose of a projectile is

$$V = \pi d^3\psi^3\left[\sqrt{\frac{1}{\psi}\left(1-\frac{1}{4\psi}\right)}\left(1-\frac{1}{3\psi}+\frac{1}{12\psi^2}\right) - \left(1-\frac{1}{2\psi}\right)\cos^{-1}\left(1-\frac{1}{2\psi}\right)\right] \tag{4}$$

where $\psi = s/d$ is the CRH for ogive projectile and s is the generatrix radius of the ogive nose. Especially for a hemi-spherical nose, we have $V = \pi d^3/12$ and $\psi = 1/2$. Assuming the volume of the original and residual noses are V_0 (correspondingly ψ_0 or s_0) and

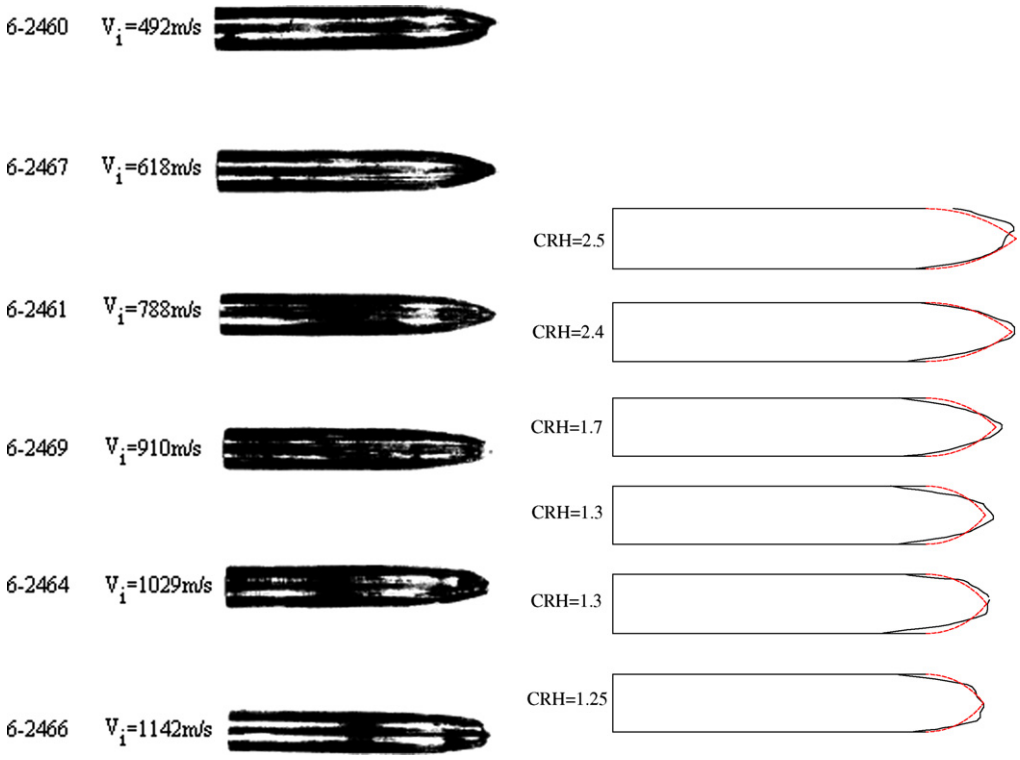

Fig. 6. Residual projectiles after penetration and the corresponding contours of nose shape(Case 2-a, CRH = 3.0)).

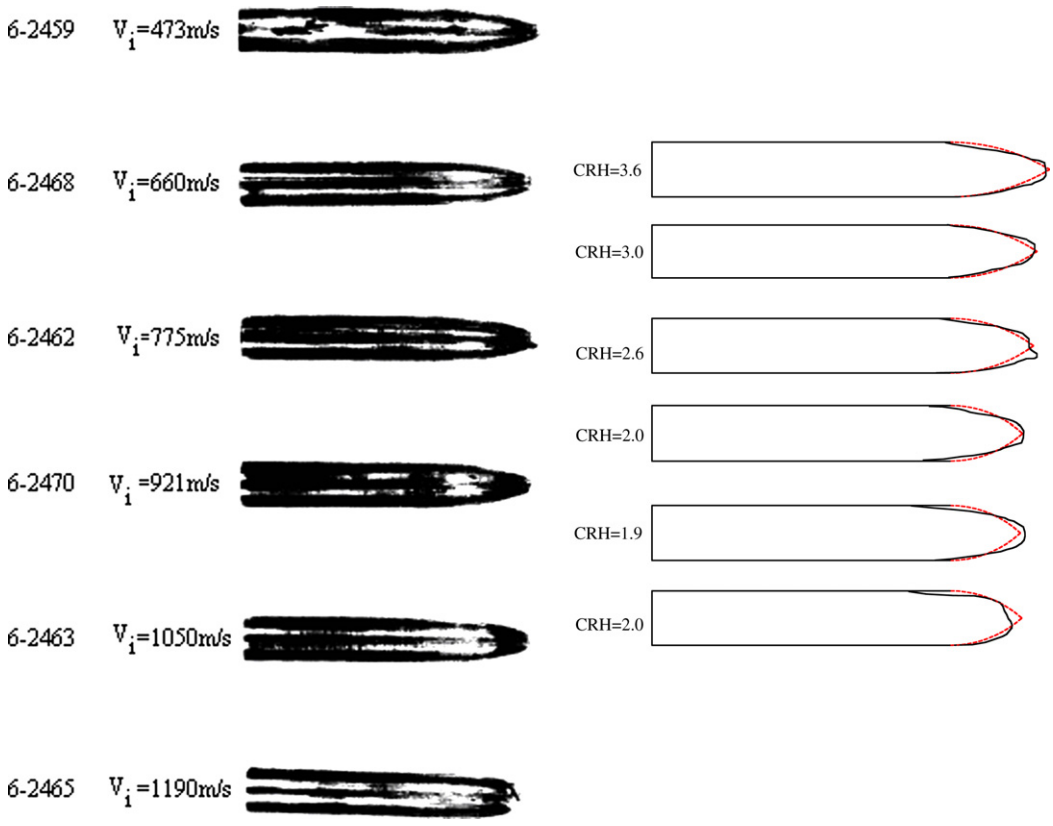

Fig. 7. Analysis on Case 2-b with CRH = 4.25 after Forrestal et al. (1996).

V_1 (ψ_1 or s_1), respectively, and the density of projectile material is ρ_p, thus the projectile mass loss is

$$\Delta M_n = \rho_p(V_0 - V_1) \tag{5}$$

In addition, the corresponding contours of the projectiles after penetrations can be drawn out according to the experimental images. Following the rule of equal vertical section area, the geometric approximation of the residual projectiles can be estimated by the closest envelope of the ogive nose, in order to determine the actual value of CRH. With the known nose shape of the original and residual projectiles, the relationship between the mass loss of ogive-nose and the variation of CRH can be obtained by Eqs. (4) and (5).

Figs. 6–11 show the residual projectiles after penetration (Forrestal et al., 1996; Frew et al., 1998) and the corresponding envelope

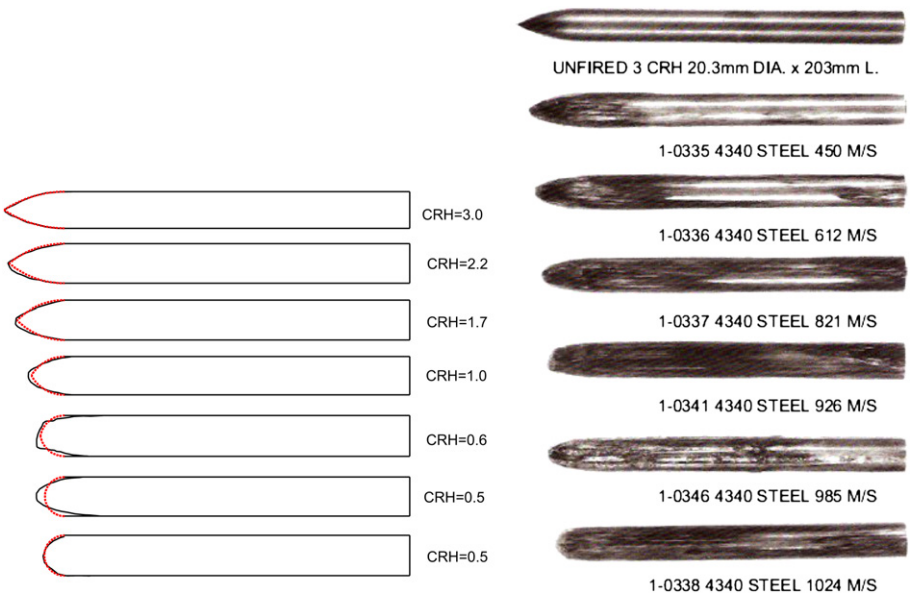

Fig. 8. Analysis on Case 3 with CRH = 3.0 after Forrestal et al. (1996).

contours of nose shapes in Cases 2–6. The shank diameters in the envelope contours are the same as the original projectiles. Case 1 is not included for the absence of its photographs. With increasing the impact velocity, the residual ogive-nose becomes much blunter and the corresponding value of CRH also becomes smaller. However, the residual ogive-nose always changes between the original geometry and a semi-spherical nose, i.e., $0.5 \leq \psi_1 < \psi_0$. In particular, the length of the residual shanks does not reduce.

Forrestal et al. (1996) and Frew et al. (1998) already estimated the total mass abrasion of each residual projectile after penetration. After determining the values of CRH according to the geometric approximation of envelope contours, Fig. 12 shows the comparison between the theoretical prediction and experimental results of the mass abrasion of projectiles with the variation of nose shape, where the two curves starting at CRH = 3 represent the hollow and solid projectiles, respectively. Excellent agreements are observed between the experimental observation and theoretical prediction. Obviously, the total mass abrasion of projectile is consistent with the mass loss of ogive-nose, i.e.,

$$\Delta M_n = \Delta M \tag{6}$$

It is further confirmed that, the mass loss on projectile shank due to high-speed friction is much less than the mass erosion on the ogive-nose due to flow erosion under extreme high temperature and pressure. The mass abrasion of a projectile mostly occurs on the ogive nose.

In the meantime, if the relations between the mass abrasion of a projectile and the initial kinetic energy [i.e. the combinations of Eqs. (1), (3) and (5)] are known, the variation of nose shape Δ(CRH) with the initial kinetic energy of a projectile can be predicted, as shown in Fig. 13. It shows that the variation of the projectile nose shape depends on the initial kinetic energy (or the initial impact velocity) and on the hardness of aggregate in concrete(Cases 3–4 and Cases 5–6). The prototype of projectile also has influence on it (Case 2-a and Case 2-b). The projectile shank type, e.g. hollow or solid shanks, also has significant influence on the variation of the projectile nose shape (Case 2-a and Cases 3–4). For each case, the variation of the projectile nose shape maintains as constant when the initial impact velocity greater than 1.0 km/s.

In conclusion, with these relations between mass abrasion and nose shape as a function of the initial kinetic energy of projectile,

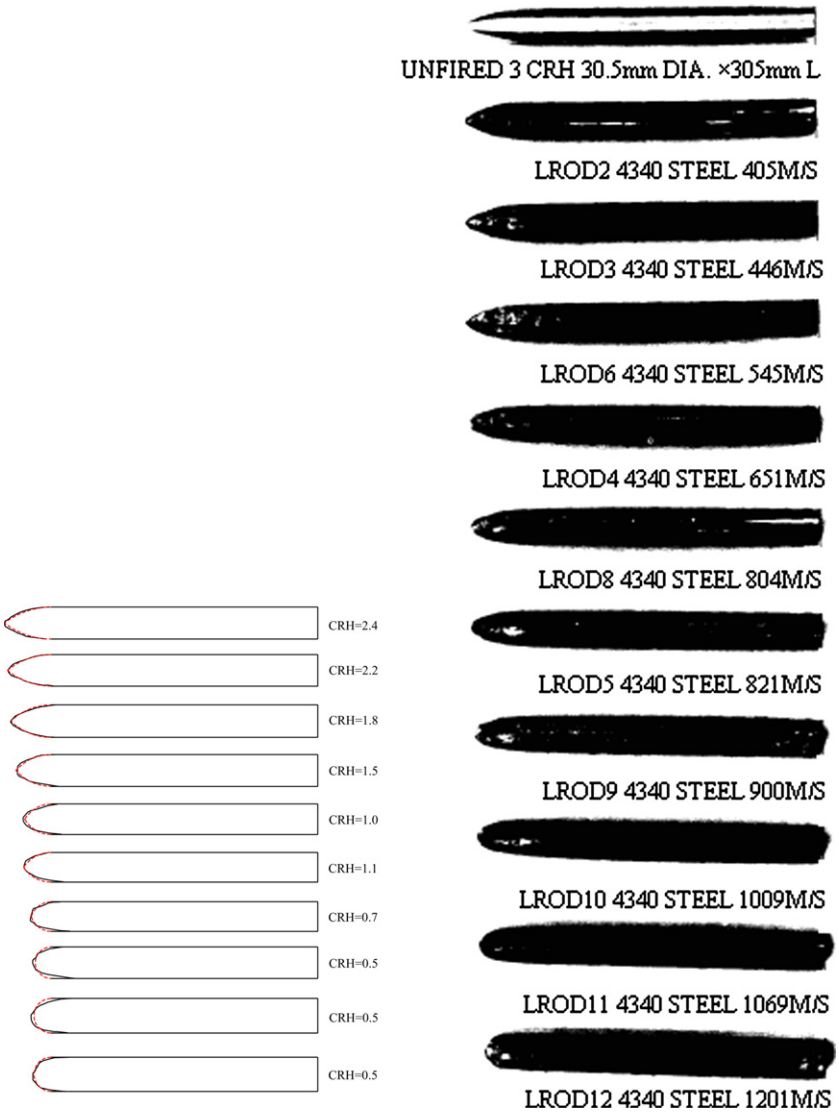

Fig. 9. Analysis on Case 4 with CRH = 3.0 after Forrestal et al. (1996).

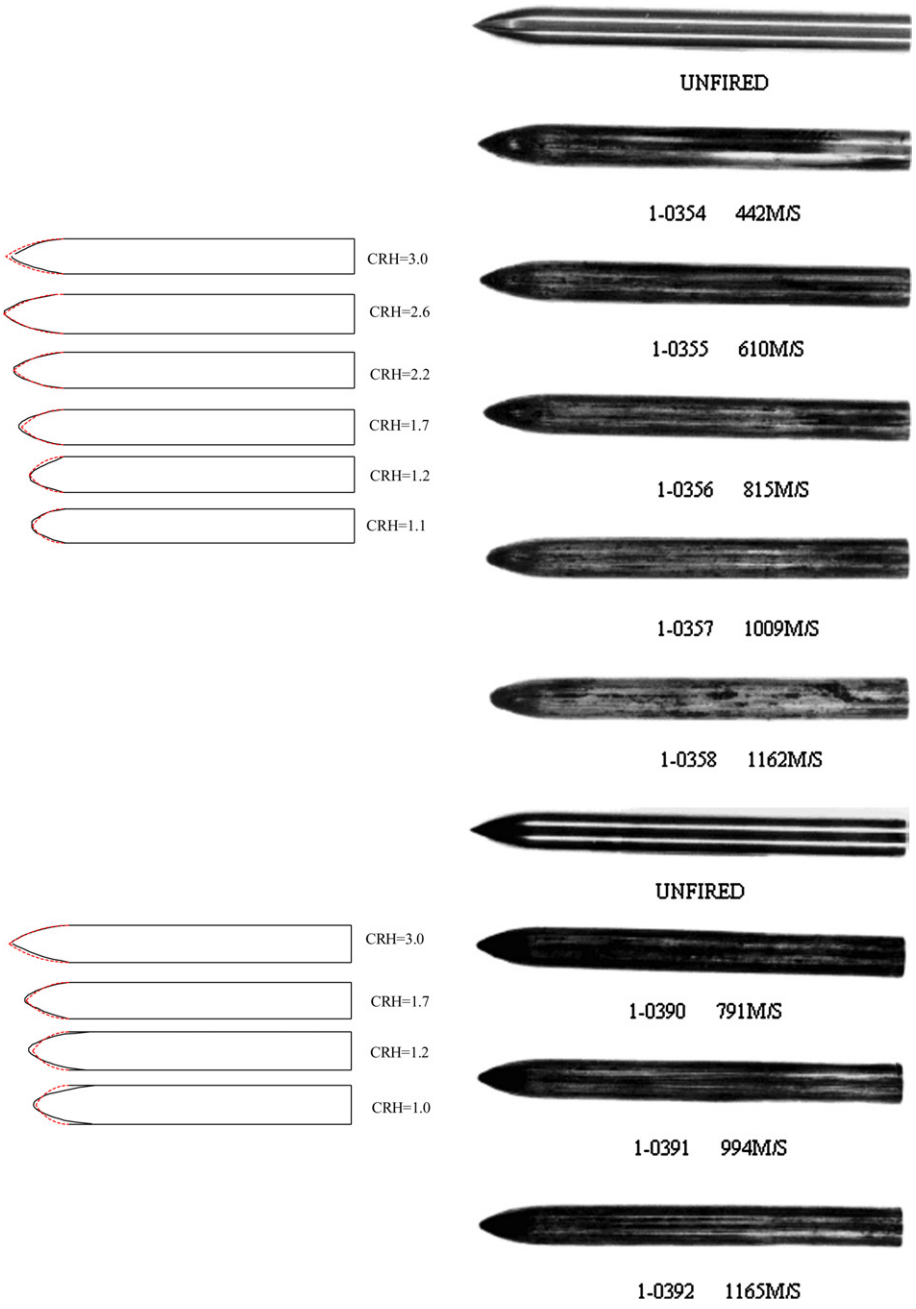

Fig. 10. Analysis on Case 5 with CRH = 3.0 after Frew et al. (1998).

one can predict these features for any impact using Eqs. (1), (3), (5) and the impact parameters (*I, N*). This empirical approach is much simpler than that used by Silling and Forrestal (2007) and Beissel and Johnson (2000, 2002).

4. The dependence of relative mass abrasion on ogive-nose

More generally, different penetrators often have different shank segments for various utilities, including variation of wall thickness, the backfilling and the geometry, etc. In contrast, the projectile nose usually is solid with limited change. The theoretical prediction in Fig. 12 already indicates the difference between hollow shank and solid projectiles. This means that some essential characteristics may be hidden to some extent if we use the definition of mass abrasion as in Section 2. For example, whether there is an upper limit of the mass abrasion of projectile with increasing impact velocity?

So it is much reasonable to use the mass of ogive-nose rather than the total mass of a projectile when we discuss the rate of mass abrasion of a projectile. Define the relative rate of mass abrasion as

$$\delta' = \frac{\Delta M_n}{M_n} = \delta \frac{M}{M_n} = \left(1 - \frac{V_1}{V_0}\right) \tag{7}$$

where δ' is only related to the values of CRH of the noses before and after penetration.

Fig. 14 shows the relation between the relative rate of mass abrasion δ' and CRH of the different initial ogive-noses. It should be pointed out that the range of CRH between 3 and 4.5 covers all

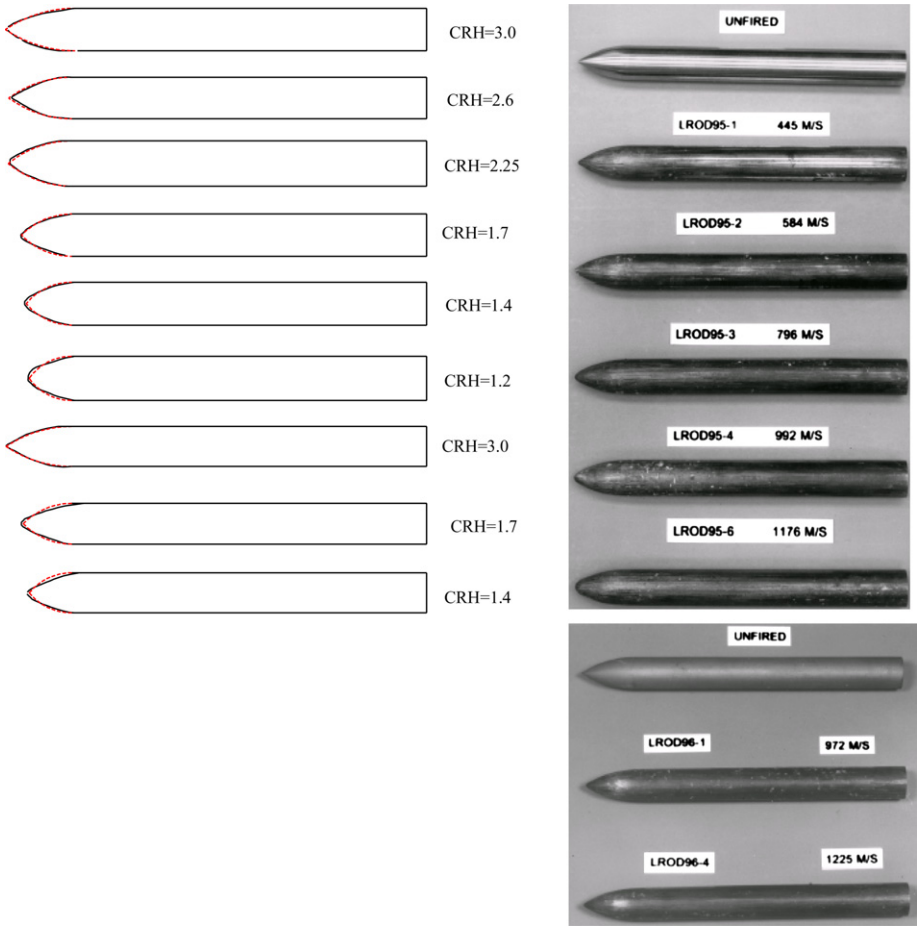

Fig. 11. Analysis on Case 6 with CRH = 3.0 after Frew et al. (1998).

possible nose shapes of deep penetrators. No matter how different the initial ogive-nose is, the relative rate of mass abrasion δ' of ogive-nose is always close to 2/3, i.e., $\Delta M_n/M_n \to 2/3$ when the ogive-nose becomes hemi-spherical, which is different from Fig. 12. Fig. 15 further depicts the relative rate of mass abrasion δ' of Forrestal et al. (1996) and Frew et al. (1998) and the corresponding theoretical prediction. Obviously, they are consistent with each other.

In a similar manner, the relations between the relative rate of mass abrasion δ' and the initial impact velocity V_i of projectile and the impact function I are shown in Figs. 16 and 17, respectively. It is well known that Cases 1–2 and Cases 5–6 are close to each other and their slopes are almost equal, and the data for cases 3–4 overlap, with another value for the slope. As indicated before, Cases 5–6 and Cases 3–4 are mainly different from the aggregate

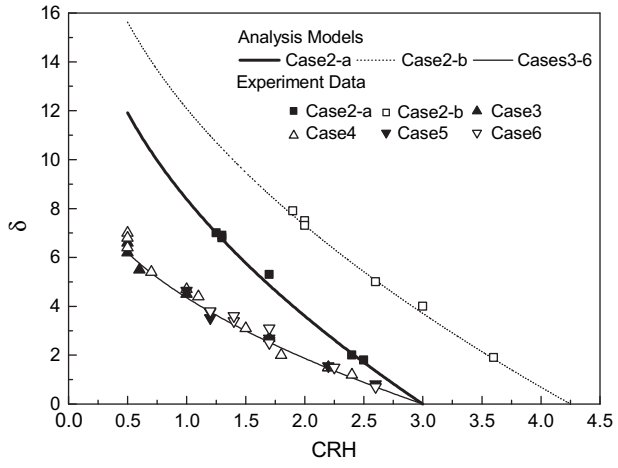

Fig. 12. Theoretical prediction and experimental results on the rate δ (%) of mass abrasion of projectiles with the variation of nose shape.

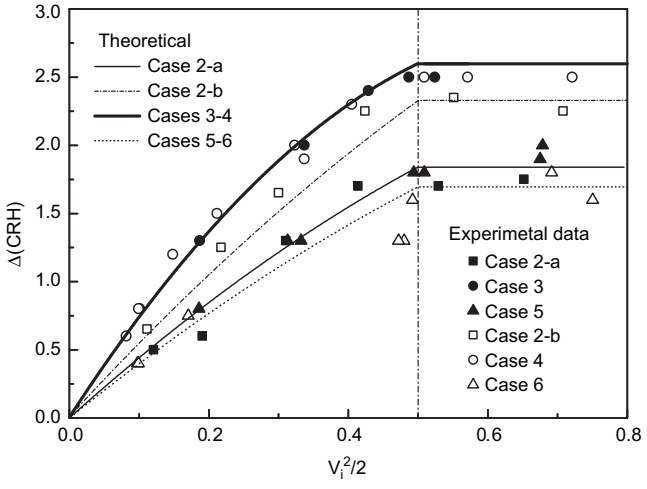

Fig. 13. The variation of CRH of projectiles before and after penetration with the initial kinetic energy.

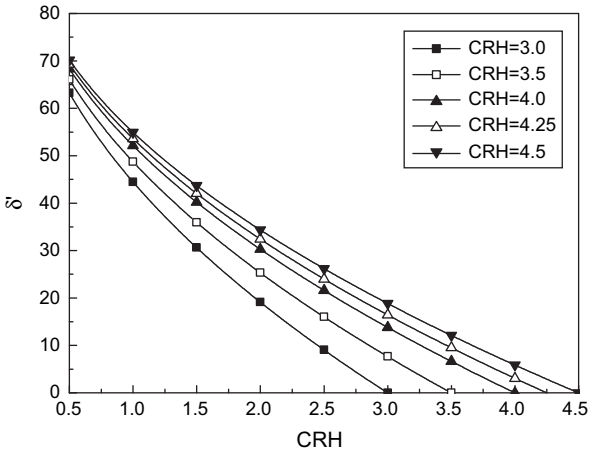

Fig. 14. The variation of relative ratio δ' (%) of mass abrasion of projectile with CRH.

hardness, i.e., $H_1/H_2 = 2.33$. According to Eq. (7) and Table 1, the distinction between Cases 1–2 and Cases 3–4 is the different mass ratio M/M_n. According to Table 1, different hollow shank projectiles are employed in Cases 1–2 and we have $M/M_n = 5.3$ and $M/M_n = 4.5$ regarding CRH = 3 and CRH = 4.25, respectively. Comparatively, solid shank projectiles are employed in Cases 3-6, where $M/M_n = 10.2$ (CRH = 3). We notice that the ratios of nose mass $\xi = 10.2/5.3 = 1.93$ or $\xi = 10.2/4.5 = 2.27$ are also close to the ratio of aggregate hardness in concretes. Therein it is easy to understand why the data of Cases 1–2 and Cases 5–6 are coincident well, and different from Cases 3–4. In other words, the projectile mass contributes to its nose abrasion. Clearly, the projectile's mass is included in its initial kinetic energy implicitly.

Furthermore, with not changing the relative rate of mass abrasion δ' of Cases 3–4, we modify δ' of Cases 5–6 by multiplying a factor $H_1/H_2 = 2.33$ as accounting for the effect of aggregate hardness, and modify δ' of Cases 1–2 by multiplying a factor $\xi = 1.93$ (CRH = 3) or 2.27(CRH = 4.25) due to the hollow shank. Therein the relations between the modified relative rate of mass abrasion δ' and the initial impact velocity V_i of projectile and the impact function I of projectile are shown in Figs. 18 and 19, respectively. Different from Figs. 16 and 17, approximately the same linear relations are observed in Figs. 18 and 19, respectively. All the

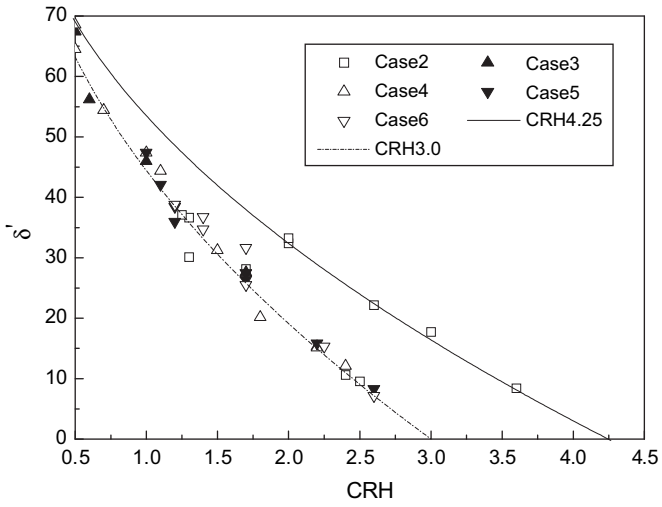

Fig. 15. Experimental results on the relative ratio δ' (%) of mass abrasion of projectile with different CRH.

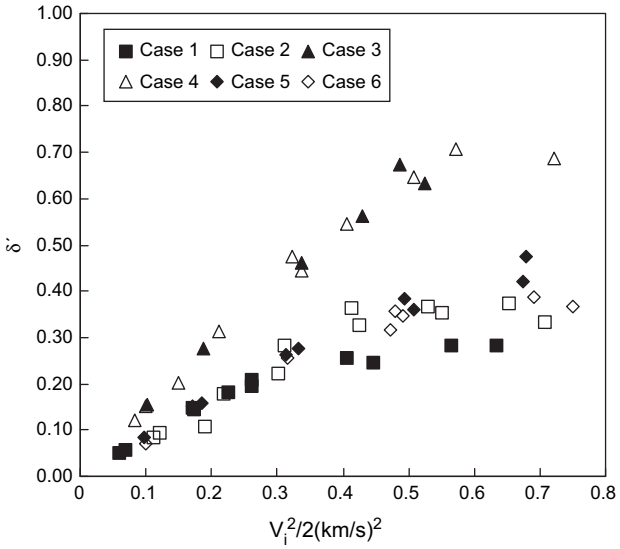

Fig. 16. Relation between the relative ratio δ' of mass abrasion and the impact velocity V_i of projectile.

data distributing coincidently with $k = 1.40$ and $C = 0.70$ in Fig. 18 and $k' = 0.007$ and $C' = 0.70$ in Fig. 19, respectively.

Unlike high-speed long rods which are used for armor ($V_i > 2$ km/s), the EPW projectiles have an explosive charge at the hollow shank, which means that structural integrity should be kept during the whole penetration process. Thus, mass abrasion should not reach the forepart of penetrator shank. We have seen that mass abrasion of these penetrators mainly occurs on the nose, and its shape varies between the initial nose shape and a hemi-spherical nose after penetration. Namely, we have,

$$\delta' \leq \frac{2}{3} \tag{8}$$

That is to say that the rate of mass abrasion δ of a deep penetrator has a theoretical upper limit,

$$\delta \leq \frac{2}{3}\frac{M_n}{M} \tag{9}$$

Regarding the solid projectiles of cases 3–6, since $M/M_n = 10.2$(CRH = 3), we have $\delta \leq 6.54\%$, which should be the

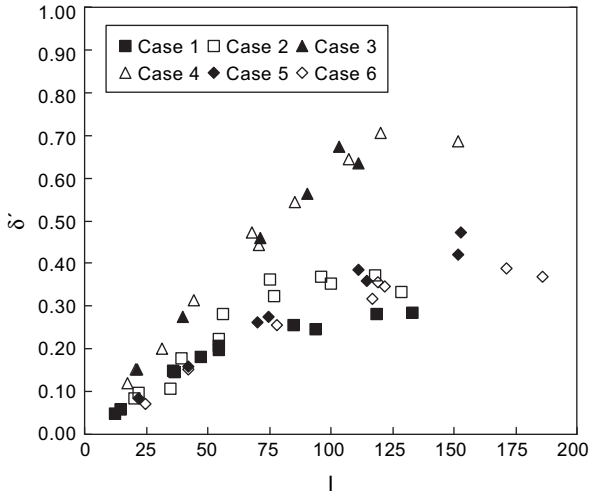

Fig. 17. Relation between δ' and the impact function I of projectile.

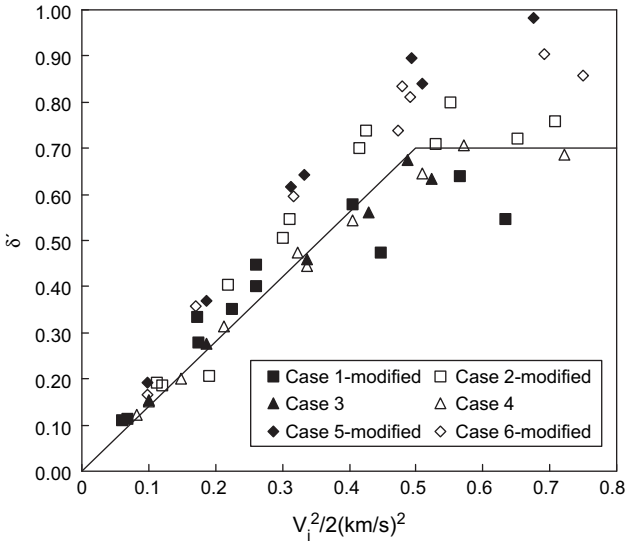

Fig. 18. Modified relation between δ' and V_i with accounting for the effects of aggregate hardness and relative mass ratio of nose.

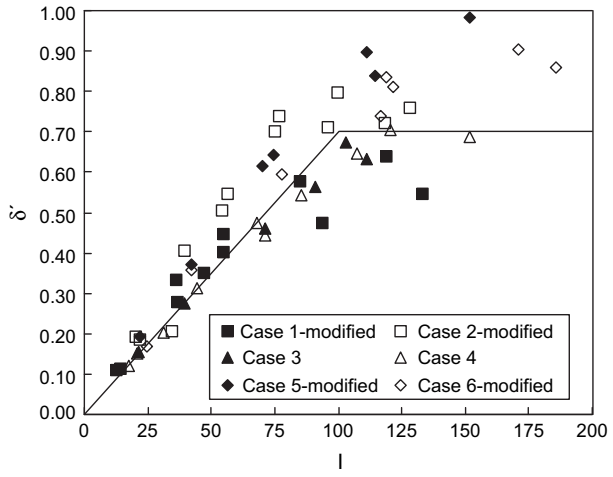

Fig. 19. Modified relation of Fig. 17 with accounting for the effects of aggregate hardness and relative mass ratio of nose.

upper limit regardless of other parameters. Similarly, for the hollow shank projectiles of Cases 1-2, we have the theoretical upper limit of $\delta \leq 12.6\%$ (CRH = 3) or $\delta \leq 14.8\%$ (CRH = 4.25). It is qualitatively consistent with the previous conclusions.

5. Conclusions

Data on mass abrasion of KE penetrators, impacting grout and concrete targets, have been examined in this paper. It is found that the projectile mass abrasion significantly depends on the initial kinetic energy (or initial impact velocity) and on the hardness of aggregate. The linear relationship between mass abrasion and initial kinetic energy is constructed after examining all the data reported by Forrestal et al. (1996) and Frew et al. (1998). The graphical analysis demonstrates that the experimental data can be normalized by using the values of the aggregate hardness. With increasing impact velocity, the nose shape will erode to a hemispherical shape which defines a theoretical limit of projectile mass abrasion. Because the mass loss mostly occurs on projectile nose, a relative mass abrasion of the ogive-nose is defined with which mass abrasion can be estimated by the variation of the nose shape, and vice versa. At the same time, a more general relation between impact function I and the projectile mass abrasion is also suggested.

Acknowledgements

The authors would like to thank Prof. Zvi Rosenberg of RAFAEL, Israel, for his careful reading of the manuscript.

References

Beissel, S.R., Johnson, G.R., 2000. An abrasion algorithm for projectile mass loss during penetration. Int. J. Impact. Eng. 24, 103–116.
Beissel, S.R., Johnson, G.R., 2002. A three-dimensional abrasion algorithm for projectile mass loss during penetration. Int. J. Impact. Eng. 27, 771–789.
Chen, X.W., Li, Q.M., 2002. Deep penetration of a non-deformable projectile with different geometrical characteristics. Int. J. Impact. Eng. 27 (6), 619–637.
Davis, R.N., Neely, A.M., Jones, S.E., 2004. Mass loss and blunting during high-speed penetration. J. Mech. Eng. Sci. Proc. Inst. Mech. Eng. 218, 1053–1062.
Forrestal, M.J., Frew, D.J., Hanchak, S.J., Brar, N.S., 1996. Penetration of grout and concrete targets with ogive-nose steel projectiles. Int. J. Impact. Eng. 18 (5), 465–476.
Frew, D.J., Hanchak, S.J., Green, M.L., Forrestal, M.J., 1998. Penetration of concrete targets with ogive-nose steel rods. Int. J. Impact. Eng. 21 (6), 489–497.
Jones, S.E., Toness, O.A., Jerome, D.M., Rule, W.K., 2001. Normal penetration of semi-infinite targets by ogive-nose projectiles, including the effects of blunting and erosion. In: Proceedings of the ASME PVP-421 Conference on Thermal Hydraulics, Liquid Sloshing, Extreme Loads and Structural Response-2001. ASME, New York, pp. 53–59.
Jones, S.E., Foster, J.C., Toness, O.A., DeAngelis, R.J., Rule, W.K., 2002. An estimate for mass loss from high velocity steel penetrators. In: Moody, F.J. (Ed.), Proceedings of the ASME PVP-435 Conference on Thermal–Hydraulic Problems, Sloshing Phenomena, and Extreme Loads on Structures. ASME, New York, pp. 227–237.
Jones, S.E., Hughes, M.L., Toness, O.A., Davis, R.N., 2003. A one-dimensional analysis of rigid-body penetration with high-speed friction. J. Mech. Eng. Sci. Proc. Inst. Mech. Eng. 217, 411–422.
Klepaczko, J.R., Hughes, M.L., 2005. Scaling of wear in kinetic energy penetrators. Int. J. Impact. Eng. 31, 435–459.
Li, Q.M., Chen, X.W., 2003. Dimensionless formulae for penetration depth of concrete target impacted by a non-deformable projectile. Int. J. Impact. Eng. 28 (1), 93–116.
Silling, S.A., Forrestal, M.J., 2007. Mass loss from abrasion on ogive-nose steel projectiles that penetrate concrete targets. Int. J. Impact. Eng. 34, 1814–1820.